A unifying principle for global greenness patterns and trends

communications earth & environment

Article

https://doi.org/10.1038/s43247-025-01992-0

A unifying principle for global greenness patterns and trends

Check for updates

Wenjia Cai [1] ✉, Ziqi Zhu[2], Sandy P. Harrison [2,3], Youngryel Ryu [4], Han Wang[2], Boya Zhou[1] & Iain Colin Prentice [1,2]

Vegetation cover regulates the exchanges of energy, water and carbon between land and atmosphere. Remotely-sensed fractional absorbed photosynthetically active radiation (fAPAR), a land-surface greenness measure, depends on carbon allocation to foliage while also controlling photon flux for photosynthesis. Here we use an equation with just two globally fitted parameters to describe annual maximum fAPAR as the smaller of a water-limited value transpiring a constant fraction of annual precipitation, and an energy-limited value maximizing annual plant growth. This minimalist description reproduces global greenness patterns and temporal trends in remote-sensing data, comparable to the best-performing dynamic global vegetation models. Widely observed greening is attributed principally to the influence of rising carbon dioxide on the light- and water-use efficiencies of photosynthesis; limited browning regions are attributed to drying. This research provides one key component of ecosystem function as a step towards more robust foundations for new-generation land ecosystem models.

The exchanges of carbon, water and energy between terrestrial ecosystems and the atmosphere are regulated by vegetation cover, often quantified by leaf area index (LAI)[1]. Plants' use of photosynthetically active radiation (PAR) for photosynthesis depends on LAI through its relationship to the fraction of PAR absorbed by leaves (fAPAR), which depends on canopy architecture[2] but can be represented at its simplest by Beer's law with a constant extinction coefficient ($k \approx 0.5$)[3]. Transpiration, tightly coupled to photosynthesis through stomatal regulation, constitutes the largest part of total global land-surface evaporation and therefore makes a major contribution to the global hydrological cycle[4]. LAI also regulates the partitioning of net surface radiation to latent versus sensible heat fluxes, exerting a first-order control on the surface energy balance—a key determinant of local and regional climates.

Global products based on optical remote sensing, representing the seasonal and interannual time course of fAPAR, are widely used as inputs to land biosphere diagnostic models. Most of these models adopt a light use efficiency (LUE) formulation, whereby gross primary production (GPP) – total photosynthesis per unit land area—over periods of a week or longer is proportional to absorbed PAR (the product of fAPAR and incident PAR)[5]. This approach can be justified theoretically as a consequence of photosynthetic acclimation, which translates the saturation response of photosynthesis to PAR – observed on sub-daily time scales—to a proportionality on time scales similar to the turnover time of Rubisco, the primary carboxylating enzyme[6]. Big-leaf models treat the canopy as a single-leaf leaf, with no differentiation between sunlit and shaded leaves. Two-leaf models allow for the differential penetration of direct and diffuse light into canopies, which results in diffuse light being used more efficiently[7–9]. Many variants of these models exist, including a two-leaf model in which the LUE of sun and shade leaves differs according to their differing radiation exposure[10]. Prentice et al.[11] reviewed current approaches and challenges associated with LUE models for monitoring GPP.

Dynamic global vegetation models (DGVMs), which form the land-surface component of many contemporary Earth System models, independently predict LAI (and thence GPP) as a by-product of the partitioning of biomass production among leaves, stems and roots. However, this partitioning is one of the less studied aspects of ecosystem function, and the existing formulations in DGVMs have not been extensively tested.

Here we explore an approach distinct from either LUE-based models or DGVMs. We seek first-order explanations for the emergence of spatial patterns and temporal trends of fAPAR in terms of eco-evolutionary optimality principles, which have been successful in explaining many features of plant and ecosystem behaviour[12]. Ground-based and remote-sensing data are used to test the hypothesis that the annual maximum fAPAR ($fAPAR_{max}$) can be represented as the lesser of two quantities: a

[1]Georgina Mace Centre for the Living Planet, Department of Life Sciences, Imperial College London, London, UK. [2]Department of Earth System Science, Ministry of Education Key Laboratory for Earth System Modelling, Institute for Global Change Studies, Tsinghua University, Beijing, 100084, China. [3]School of Archaeological, Geography and Environmental Sciences, University of Reading, Reading, UK. [4]Department of Landscape Architecture and Rural Systems Engineering, Seoul National University, Seoul, 08826, South Korea. ✉e-mail: w.cai17@imperial.ac.uk

water-limited value and an energy-limited value. The water-limited value is determined by the principle of 'ecohydrological equilibrium', which states that a fixed fraction of antecedent annual precipitation is available to support photosynthesis[13]; the energy-limited value maximizes plant growth by balancing the benefit of photosynthesis against a cost, which is assumed to be proportional to LAI. Conceptually, this cost comprises the construction and maintenance costs of leaves, plus the additional carbon allocation required to keep the leaves supplied with water and nutrients. Our approach was first applied to the Tibetan Plateau[14] and used to explain observed, divergent responses of energy- and water-limited vegetation to recent environmental changes. which paved the way for the present, global application.

Implementation of this hypothesis is facilitated by the use of the P model[6,15,16], a universal, first-principles LUE model for GPP that has no free parameters and requires no plant functional type (PFT) distinctions apart from the separation of C_3 and C_4 photosynthetic pathways (see Online Methods). The P model has been tested extensively against eddy-covariance-based estimates of GPP across biomes[7,15]. Based on the broad concept of eco-evolutionary optimality[7], the P model assumes that vegetation is adapted and/or acclimates to environmental changes in a way that minimizes the combined biochemical and water-transport costs associated with photosynthesis while also maintaining biochemical capacity at just the right level to use all of the available light[6]. These assumptions make it possible to dispense with the need to estimate different sets of parameters for different PFTs, thus removing a key source of uncertainty in remote-sensing-based GPP models[11].

The P model has the convenient mathematical form of a LUE model, resulting in proportionality between fAPAR, GPP and transpiration[17]. Our analysis here extends the principles underlying the P model to allow independent prediction of the annual maximum fAPAR. Under water limitation, optimal fAPAR is taken to be the value that transpires a globally invariant fraction (to be estimated from data) of antecedent annual precipitation. This is optimal in the sense that plants are thereby assumed to adapt their rooting strategy to make use of annual precipitation, whatever its temporal distribution. Under energy limitation, optimal fAPAR is taken as the value yielding the largest excess of annual GPP over the canopy cost, which is assumed to be proportional to LAI (see online Methods). Optimization of LAI is assumed to be independent of leaf mass-per-area (LMA), as co-existing plant species typically vary substantially in LMA, yet those with higher LMA do not display lower LAI[18]. We use remotely-sensed fAPAR rather than LAI as the quantity for direct comparison with model results in order to avoid problems associated with the saturation of reflectance at high LAI values, where fAPAR approaches unity[19]. We focus on the annual maximum value of fAPAR per 0.5°; grid cell and year ($fAPAR_{max}$) as plants must allocate enough carbon to foliage to achieve this maximum, and specifically on the 95th percentile of the distribution of $fAPAR_{max}$ within each grid cell in order to minimize the effects of disturbance or land management. We do not consider phenology, which can, however, be separately predicted (given an annual maximum LAI) based on the seasonal time course of potential GPP[20].

This modelled annual maximum fAPAR reproduces global greenness patterns, and the consistent temporal trends among remote-sensing products, as accurately as the best-performing dynamic global vegetation models. Widely observed greening is attributed to the influence of rising carbon dioxide on the light- and water-use efficiencies of GPP, augmented by wetting in some dry regions and warming in high latitudes. Limited regions show browning, attributed to drying.

Results

Global comparisons to in situ data and spatial patterns

Ground-based measurements of green vegetation cover apply to small areas and can therefore be subject to large variation related to local soil conditions and disturbance history. Reasonable agreement was nonetheless obtained between a composite set of ground-based fAPAR[21,22] and our predictions (Fig. 1). Mismatches were predominantly overpredictions, particularly in

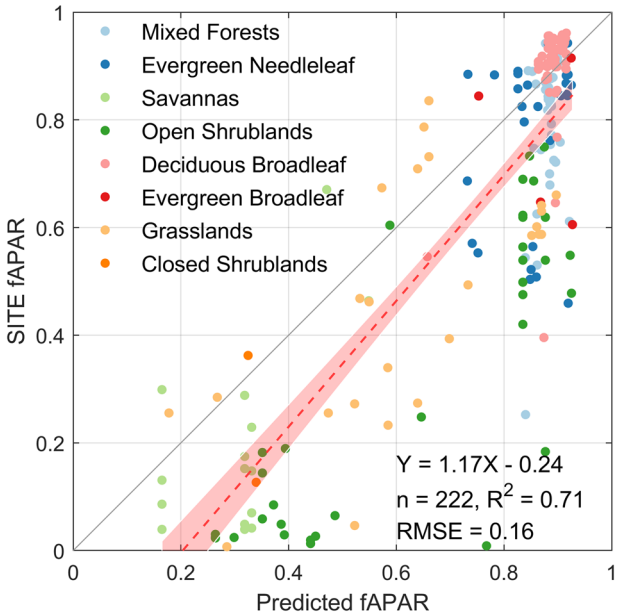

Fig. 1 | Comparison of predicted fAPARmax with observations. Predictions are from the theoretical model driven by environmental variables. Observations are from the GBOV and OLIVE datasets. Observed biomes are shown with different colours; the model is incognizant of biome type. The dashed line is the regression line, with the red shaded area being the 95% confidence interval; the solid line is the 1:1 line. RMSE, root-mean-squared error of prediction; n, number of observations; R^2, proportion of observed variance accounted for by the prediction.

shrublands; the observed values are bounded above by a line close to the 1:1 line between observations and predictions. The geographic pattern of $fAPAR_{max}$ predicted by this simple approach shows good agreement with the observed global pattern derived from MODIS data[23] (Fig. 2). The differences between modelled and observed multiyear average fAPAR (mod–obs; Fig. S1) were commonly (53%) within ± 0.1, and most (72%) differences were within ± 0.15. Larger underestimation occurred in the Sahel region of Africa, the caatinga region of north-eastern Brazil, and south-western North America. Large overestimation is evident in the Tibetan Plateau and some other, smaller regions at high latitudes or altitudes, such as northeast Greenland and the high Andes (Fig. S1).

We compared the performance of our model with that of 15 DGVMs participating in the TRENDY project[24] version 9 (Table 1; Fig. 3). Our predictions performed as well as the best of the TRENDY models on the three criteria of R^2, slope of the regression of observed versus modelled annual maximum fAPAR, and root-mean-squared error (RMSE)—achieving the highest R^2 (0.95) tied with two other models (the model range is from 0.76 to 0.95), a regression slope within ± 0.02 of unity along with only four other models (the model range is from −0.18 to +0.13), and a low RMSE (0.15) equalled or marginally outperformed by only three other models (the model range is 0.14 to 0.33).

We also conducted sensitivity tests on values for z, f_0 and k to examine the degree to which variations in these parameters can influence our model performance and whether adopting constant values would result in sufficiently robust predictions. The model with temperature-dependent z and f_0 produced a higher R^2 (0.97) and regression slope (almost 1) and reduced RMSE (0.12), making it the best-performing of all models (Fig. S2). Using either a spatially varying field of k values, or vegetation type-specific values (Fig. S3 & Tab. S1), resulted in only marginally different estimates of z and f_0 (Tab. S2) and slight deteriorations of the goodness of fit of the model (Fig. S4). Using MODIS-derived k yielded slopes closer to 1 but with a high RMSE, possibly due to the occurrence of a few unrealistically high values (>1000) for k estimated in this way. MODIS-derived k values were less dispersed when reduced to vegetation type-specific medians, leading to reduced RMSE (Fig. S4c). Predictive skill was similar whether using

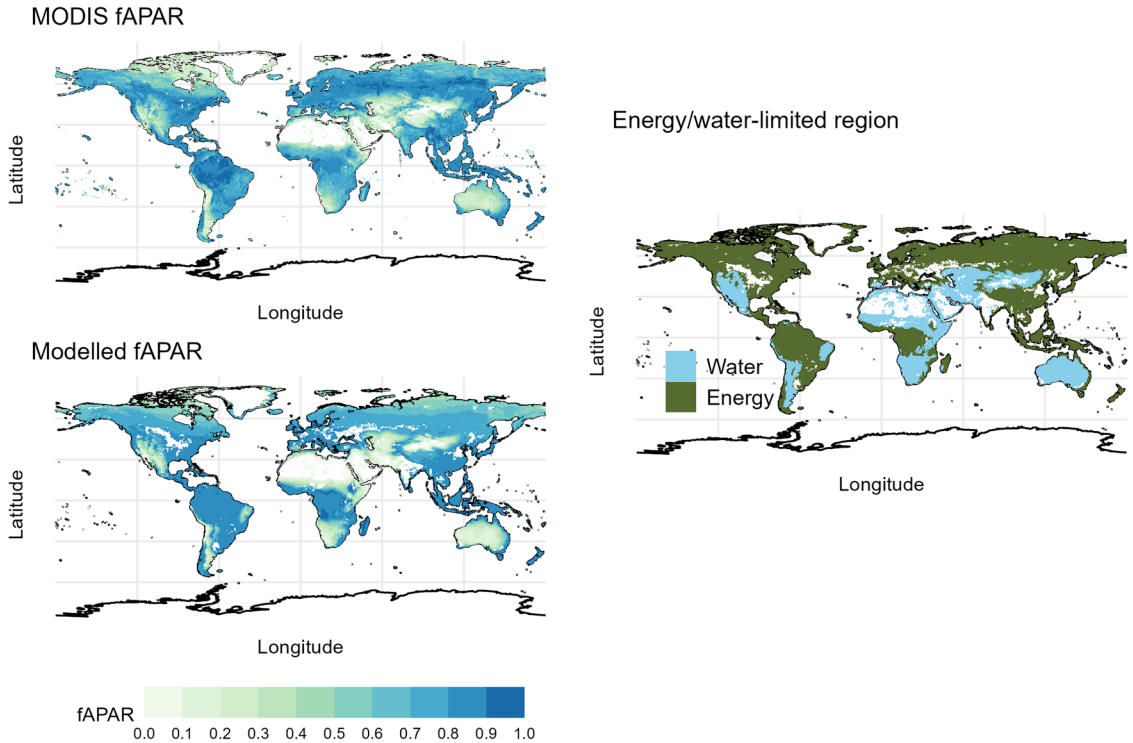

Fig. 2 | Comparison of the spatial distribution of simulated and observed annual maximum fAPAR from the P model (bottom left) and MODIS observations (top left). Energy- and water-limited regions are shown in the middle right panel. Simulated and observed annual maximum fAPAR are multi-year averages for the study period of 2000–2017.

vegetation type-specific k values inferred from MODIS, or from in situ measurements (Fig. S4c, d). The best overall performance was achieved by the model with constant k.

Trends during the satellite era

Temporal trends in observed and modelled $fAPAR_{max}$ during 2000–2017 were represented by non-parametric Mann-Kendall coefficients (see Online Methods). The evaluation of modelled temporal trends is hindered by relatively large and generally unexplained differences among remotely sensed products. Nonetheless, after eliminating grid cells where fitted trends showed opposite signs in different products, we simulate the major features of observed trends (Fig. 4). Widespread greening was both observed and modelled. However, parts of semi-arid Central Asia and southwestern Africa, coastal California, the caatinga region of north-eastern Brazil and interior Argentina, showed browning trends both in observations and in the model. Nonetheless, 27% of natural vegetated land showed greening, whereas less than 6% experienced browning. The model achieved a level of success in reproducing temporal trends comparable with that attained by the best-performing TRENDY models (Fig. 5). R^2 values greater than that obtained with the P model (0.37) were achieved by 40% of the TRENDY models. However, among these, our model uniquely approached a regression slope of 1 (0.81); other models had regression slopes of 0.63 or less. Across all models, R^2 values ranged from 0.13 to 0.46, and regression slopes from 0.45 to 0.81. RMSE values were similar (0.29 to 0.37) across all models.

Quadratic polynomials and bent-cable piecewise linear regression were used to examine the possibility of shifts in fAPAR trends (see Online Methods). Quadratic regressions of the global average annual maximum fAPAR trend were less significant ($p = 0.055$) than simple linear regression ($p = 0.034$) while ANOVA showed that quadratic regression was not better than linear regression ($p = 0.24$). When this test was applied to each grid cell, the majority of grid cells (~91%) showed the same results except for limited regions in Amazonia, southern Argentina, central Asia and some parts of Africa (Fig. S5). Bent-cable regression indicated that the number of grid cells showing hat-shaped trends, which showed an initially increasing annual maximum fAPAR followed by declining trend, exceeded the number showing cup-shaped (first negative then positive) trends, although throughout the whole period these regions exhibit mostly positive trends (Fig. S6 & Fig. 4). A very few grid cells (mainly in the Mediterranean region and north-eastern Brazil) showed a continuing decrease. Hat-shaped trends were widely distributed but a significant portion of these shifting trends showed turning points close to the start of the period (Fig. S6a), casting doubt on their reliability.

For grid cells where most remotely sensed products agreed on the sign of the temporal trends, we estimated the dominant control of the trend (Fig. 6) by performing multiple simulations in which each environmental variable was held constant in turn to assess its influence (see Online Methods). Rising CO_2 was implicated as the dominant cause of greening trends over much of the world, in agreement with previous analyses[25]. However, substantial areas showed greening trends that the model attributed to increasing precipitation, while smaller areas (including those listed previously) showed browning trends that the model attributed to declining precipitation. Increasing temperature is indicated to have led to greening in some regions of the northern high-latitudes, but to browning in a few other locations[20]. There are also regions, for example in parts of India and China, where observed greening has been stronger than our model predicts. This is likely due to direct human influence in the form of agricultural intensification, and (in China) reforestation[26].

Discussion

Our top-down approach intentionally glosses over potentially important details, such as the likelihood of environmental influences on f_0 and z. Under water limitation, we have simply assumed that plants can access a fixed fraction of precipitation, adapting their root-zone capacity as needed to ensure this even in highly seasonal climates. Some theoretical work has pointed to an optimality constraint on this fraction, acting via the coordination of stomatal and hydraulic traits[27]. Yang et al.[28] postulated the existence of a maximum 'rain use efficiency' and found, through an analogy with the Budyko curve, that high fAPAR sharpened the transition between

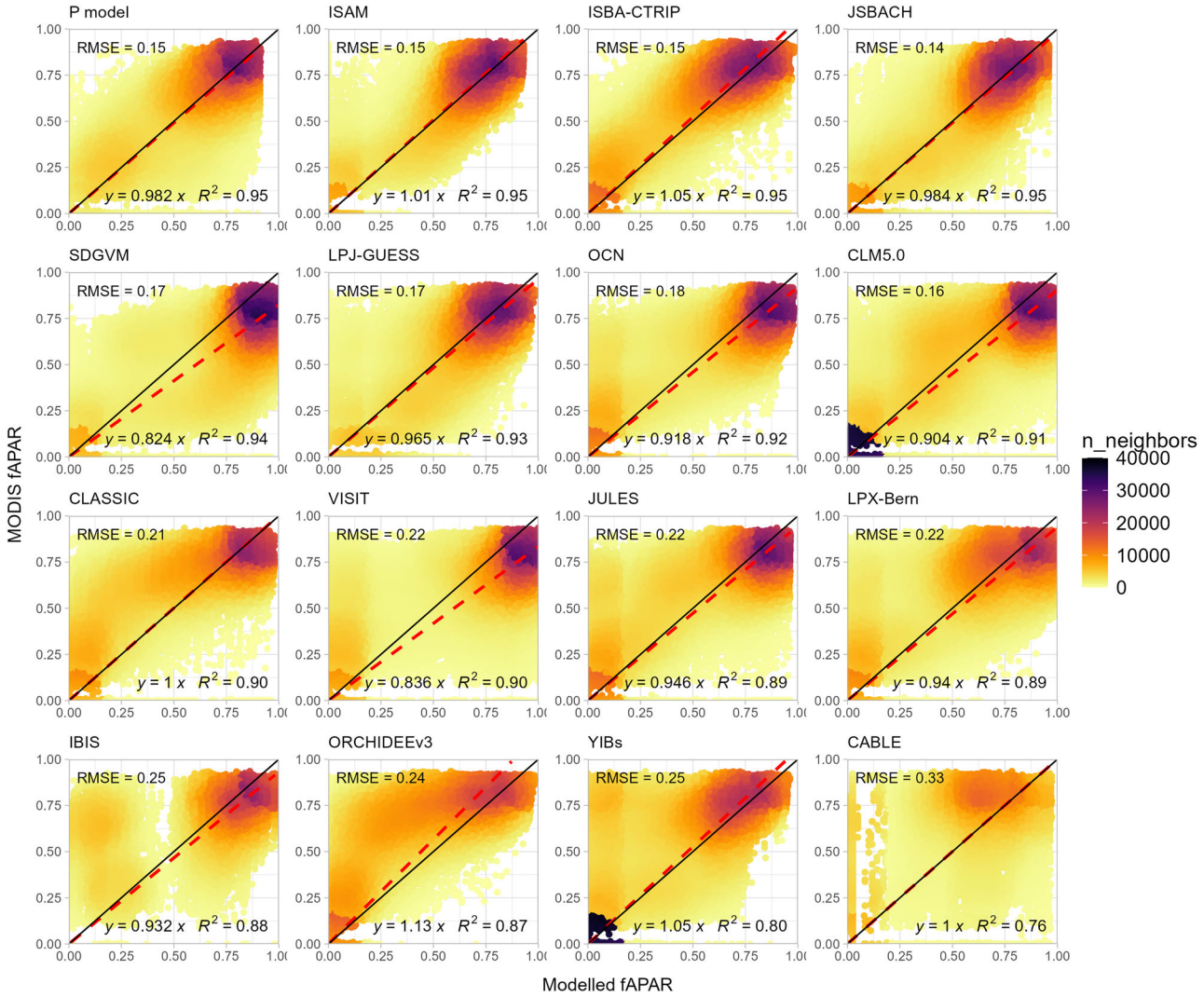

Fig. 3 | Comparison of simulated fAPARmax and observed fAPARmax from MODIS. The red dashed line is the regression line; the black solid line is the 1:1 line. RMSE: root-mean-squared error of prediction; R^2: proportion of observed variance accounted for by the prediction; n_neighbors: number of neighboring points around each point.

energy and water limitation of GPP. Under energy limitation, we have assumed a fixed cost factor z for the maintenance and replenishment of the canopy. However, these factors are also likely to vary with environmental factors, including growth temperature, growing-season length and aridity[29] as well as aspects of soil fertility, as less fertile soils are likely to induce higher costs in below-ground allocation for the uptake of nutrients[30].

Over- and under-estimation of fAPAR compared to observations was primarily a result of adopting constant values for z and f_0. The z value fitted globally (13.86 mol C m^{-2} a^{-1}) was lower than that fitted specifically to data from the Tibetan Plateau[14] (> 25 mol C m^{-2} a^{-1}). Estimated values for z are shown to rise towards areas with lower temperatures. Such a trend would account for higher z being required to estimate fAPAR accurately in cold regions, including the Tibetan plateau, where our current analysis systematically overestimates fAPAR. Plant-available water might be expected to be lower in dry areas, so it is not surprising that some of the highest biases occurred in arid and semi-arid regions (Fig. S7).

Our attempt to fit values of the two model parameters against growth temperature revealed different responses. f_0 shows a nearly monotonic positive increase with temperature. z declines with increasing temperature up to about 12 °C, followed by an increase, then a further decrease after about 21 °C (Fig. S8). The increasing relationship between f_0 and temperature is consistent with previous research[31] suggesting increasing

Table 1 | Details of the models from TRENDY-v9

Model name	Spatial resolution	Reference
CABLE-POP	1° × 1°	Haverd et al.[63]
CLASSIC	2.8125° × 2.8125°	Melton et al.[64]
CLM 5.0	0.9375° × 1.25°	Lawrence et al.[65]
IBIS	1° × 1°	Yuan et al.[66]
ISAM	0.5° × 0.5°	Meiyappan et al[67]
ISBA-CTRIP	1° × 1°	Delire et al.[68]
JSBACH	1.875° × 1.875°	Reick et al.[69]
JULES-ES	1.25° × 1.875°	Wiltshire et al.[70]
LPJ-GUESS	0.5° × 0.5°	Smith et al.[71]
LPX-Bern	0.5° × 0.5°	Lienert and Joos.[72]
OCN	1° × 1°	Zaehle and Friend.[73]
ORCHIDEEv3	0.5° × 0.5°	Vuichard et al.[74]
SDGVM	1° × 1°	Walker et al.[75]
VISIT	0.5° × 0.5°	Kato et al.[76]
YIBs	1° × 1°	Yue and Unger.[77]

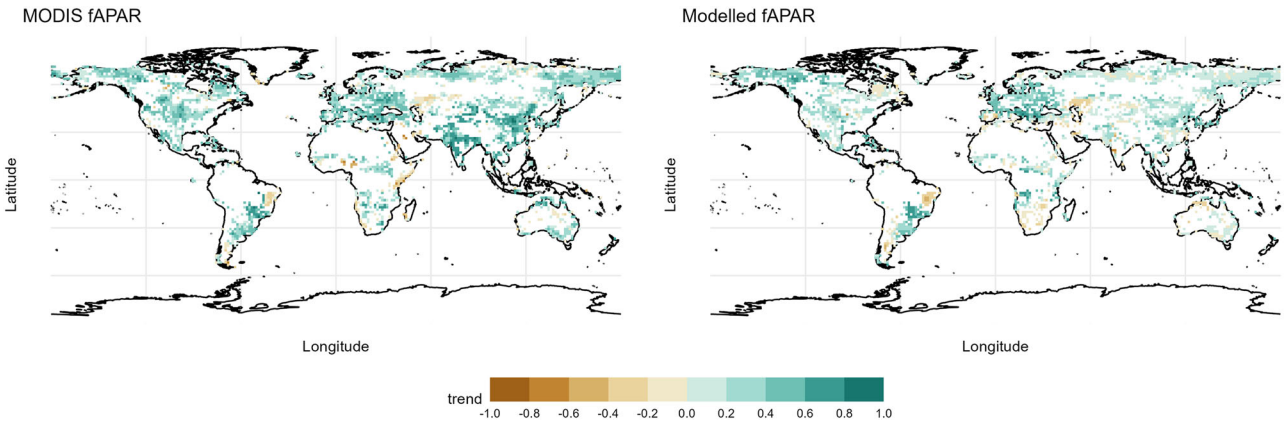

Fig. 4 | Trends in annual maximum fAPAR derived from the P model and from MODIS observations. fAPAR trends were quantified using Mann-Kendall coefficients. Regions with high fAPAR (>0.85) in the initial year, or where remotely-sensed products disagree on the sign of the trend, are excluded.

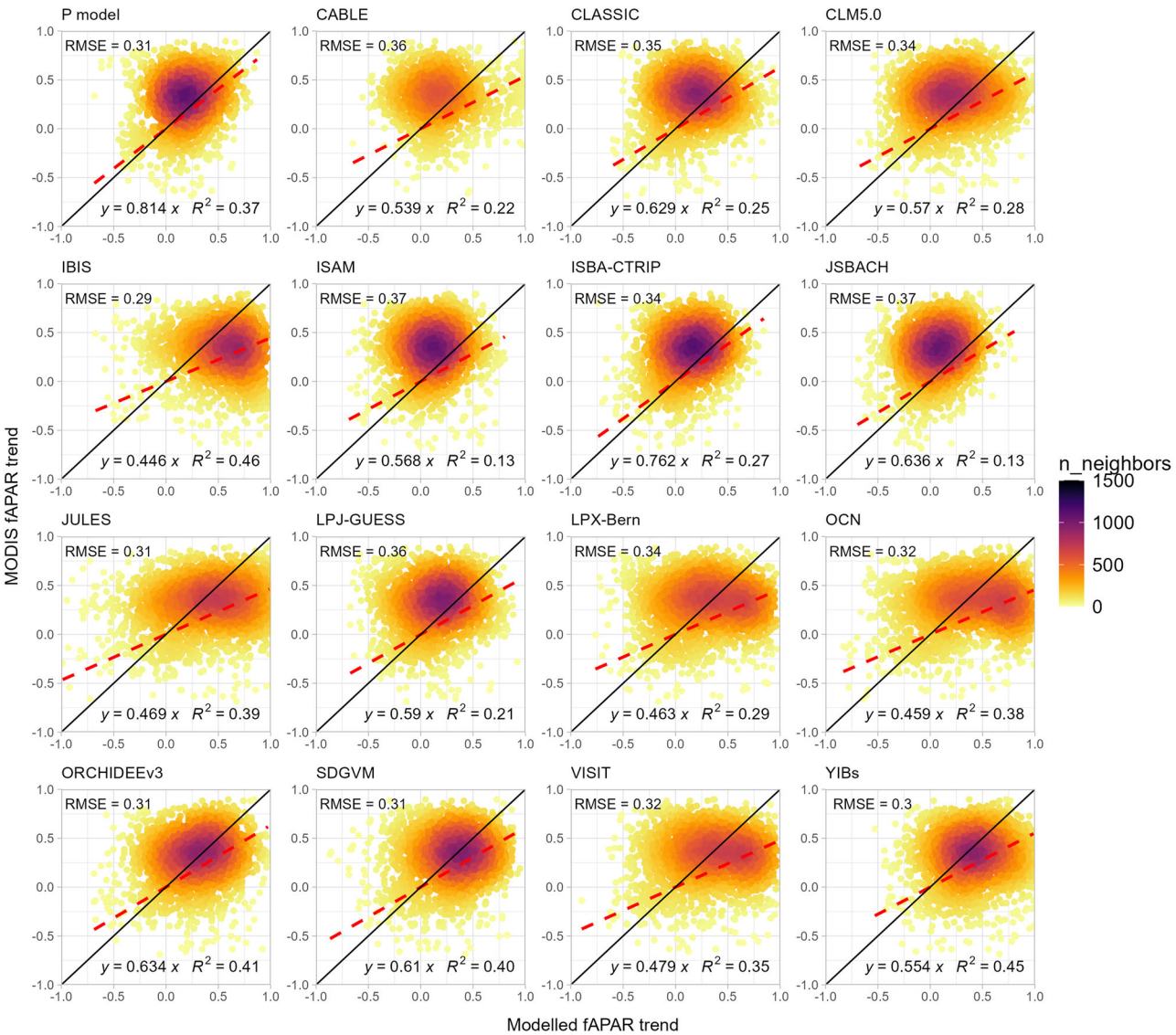

Fig. 5 | Comparison of simulated and observed trends in fAPARmax. The simulated trends are derived from the P model and the 15 models participating in the TRENDY project. The observations are derived from MODIS. Red dashed line is the regression line; black solid line is 1:1 line. RMSE: root-mean-squared error of prediction; R^2: proportion of observed variance accounted for by the prediction; n_neighbors: number of neighboring points around each point.

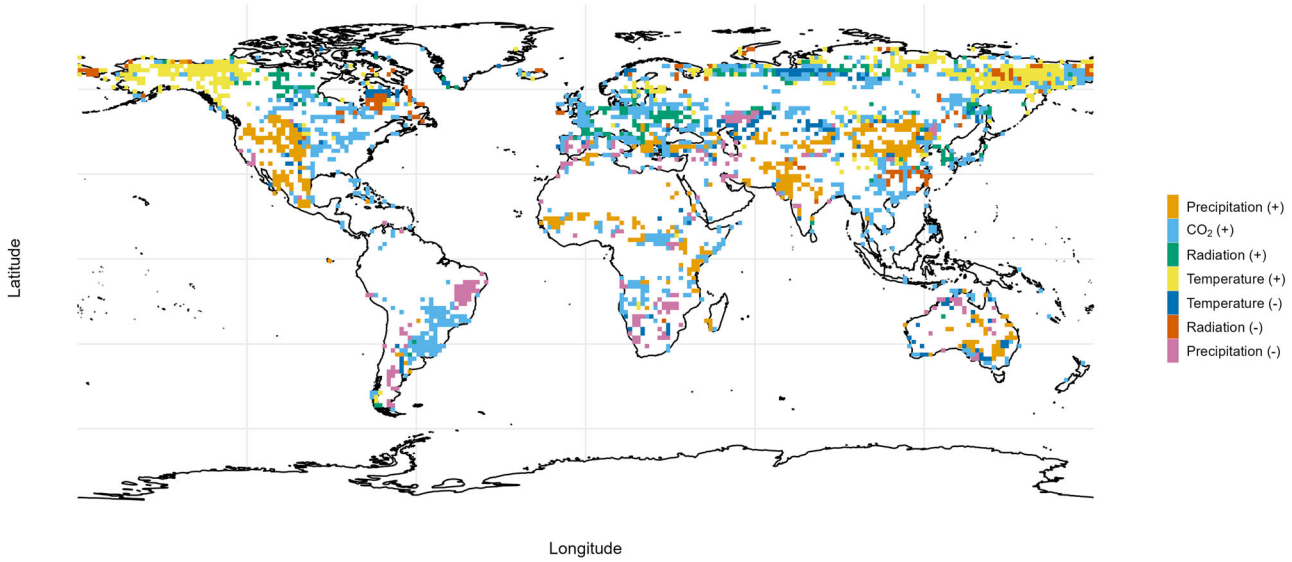

Fig. 6 | Identification of the dominant driver of the trend in P-model simulated annual maximum fAPAR, where (+) and (−) indicate a positive or negative effect of each driver. Regions with high fAPAR (>0.85) in the initial year, or where remotely-sensed products disagree on the sign of the trend, are excluded.

vegetation water uptake at higher temperatures. A possible explanation for the initially decreasing, then increasing relationship of z to temperature might be that nutrient limitation at the low end is alleviated by rising temperature, allowing less below-ground allocation per unit leaf area[32], while water limitation under warmer climates is exacerbated by rising temperature, forcing plants to allocate more below ground. This is broadly consistent with the pattern shown in Ma et al.[33] whereby the relationship of forest root mass fraction to temperature is positive on dry soils but negative on wet soils. Adopting the empirical temperature dependency of z and f_0 improves model performance to some extent (Fig. S2). Such dependencies would repay further study both from a theoretical standpoint and in remotely sensed observations. Nonetheless, the fidelity of our minimalist model to the major spatial and temporal patterns in fAPAR data is notable, as is its ability to reproduce both aspects as well as or better than the far more complex DGVMs.

Ecohydrological optimality concepts have a long but chequered history. Some specific hypotheses earlier proposed by Peter Eagleson, a pioneer of global ecohydrology, are now considered implausible from an eco-evolutionary perspective[34,35]. A link has been noted between the ratio of transpiration to precipitation (equivalent to f_0) and the aridity index (AI, the ratio of potential evapotranspiration to precipitation)[31]. According to Good et al.[36], f_0 has a unimodal relationship to AI, reaching a maximum value at an AI around 1.5. The ascending limb of this relationship relates to our energy-limited case, with fAPAR independent of precipitation. The maximum of f_0 reported in Good et al.[36] is about 0.6, close to our fitted value for water-limited regions. The descending limb corresponds to a decline in f_0 with increasing aridity. Here, however, we have intentionally kept the formulations as simple as possible, to illustrate general principles and to facilitate comparison with previous studies. By linking remotely sensed data with theory in this way, we anticipate that this work will contribute to the development of more comprehensive theory for the interactions of vegetation and its growth environment.

The canopy extinction coefficient (k) depends on canopy structure, particularly the leaf angle distribution[37,38]. It has long been observed (and theoretically predicted) that more vertically inclined leaves, as in needleleaf forests, lead to lower values of k whereas more horizontally inclined leaves, as in broadleaf forests, lead to higher values of k[38,39]. In addition, high fAPAR appears to favour low k, allowing more efficient penetration of light into dense canopies. Hikosaka and Hirose[38] proposed the existence of an optimal k dependent on vegetation density, which could explain the geographic pattern in apparent k and might also imply temporal variation in k. Indeed, declining k towards the peak growing season, which would enable greater light penetration, has been noted[40]. However, our analysis has shown that the specification of k is not critical to determining the geographic patterns or temporal trends in fAPAR, which are predicted with reasonable accuracy assuming an invariant k.

Both positive and negative trends in vegetation greenness in recent decades have been reported. Negative trends have mostly been associated with intensified drought stress accompanying warming[41,42]. However, our analysis does not support a general transition from greening to browning from 2000 onwards. Rather, it supports the hypothesis that potential negative effects of increasing temperature and vapour pressure deficit have generally been more than counterbalanced by the positive effects of rising atmospheric CO_2 concentration, and of longer and warmer growing seasons in high latitudes[25]. Weakening or negative trends of primary production diagnosed in some research might be due to lack of consideration of CO_2 fertilization effect in light use efficiency (LUE)[43]. Given the accelerated rate of warming and further interactions between environmental drivers, however, there are likely to be shifts in future predictions of leaf area that could counteract the positive effects of rising CO_2[44].

This research has potential utility in providing one key component of a general optimality-based model for ecosystem function. Current global land models contain many ad hoc and untested 'legacy' elements – not least for the determination of carbon allocation to roots, shoots and leaves, for which there are few generally accepted principles. If the tendency of fAPAR can be predicted (and the costs of LAI quantified in terms of required below-ground allocation), it should be possible also to predict annual carbon profit – and thereby formulate an evolutionarily stable strategy for height competition among plants[45]. These elements are all required, if a new generation of land ecosystem models is to rest on more secure foundations.

Methods

Optimality criteria

For C_3 plants, the optimality equations (see Online Methods for derivations) are:

$$fAPAR_{\max} = f_0\, P\, ca\,(1-\chi)/(1.6D\, A_0) \quad (1)$$

under water limitation and

$$fAPAR_{\max} = 1 - z/(k\, A_0) \quad (2)$$

under energy limitation, where $fAPAR_{max}$ is annual maximum fAPAR (assumed in (2) to be related to annual maximum LAI via Beer's law,

$fAPAR_{max} = 1 - \exp(-k\ LAI_{max})$ with $k = 0.5$), f_0 is the fraction of annual precipitation (P, mol m^{-2} a^{-1}) available for uptake by plants, c_a is the ambient partial pressure of CO_2 (Pa), χ is the ratio of leaf-internal to ambient CO_2, D is the vapour pressure deficit (vpd, Pa), z is the cost factor for LAI, and A_0 is the potential GPP (mol C m^{-2} a^{-1}), i.e. the GPP that would be achieved if $fAPAR_{max} = 1$. The term χ is a function of growth temperature, vpd and atmospheric pressure, while A_0 is a function of incident PAR, temperature and χ. Single, global values of the two free parameters (f_0 and z) were estimated by non-linear regression using the log-sum-exp approximation to the minimum function (Note S1).

The P model

We used the P model[6,15,16] to provide the components of Eqs. (1) and (2). The P model is based on the Farquhar-von Caemmerer-Berry photosynthesis model, but has the mathematical form of a LUE model. It simulates terrestrial ecosystem gross primary production (GPP) as a function of atmospheric CO_2 concentration, air temperature, atmospheric pressure, vapor pressure deficit (vpd, expressed as D), incident photosynthetic photon flux density (PPFD), the fraction of incident PPFD absorbed by vegetation (fAPAR), root-zone soil moisture (θ) and C_4 vegetation fraction as follows:

$$A = \varphi_0 . PPFD . fAPAR . m\sqrt{\left[1 - \left(\frac{c^*}{m}\right)^{2/3}\right]} \quad (3)$$

where

$$m = \left(c_a - \Gamma^*\right) / \left\{c_a + 2\Gamma^* + 3\Gamma^*\sqrt{\left[1.6\eta^* D\beta^{-1}(K + \Gamma^*)^{-1}\right]}\right\} \quad (4)$$

Here, φ_0 is the intrinsic quantum yield estimated following Bernacchi et al.[46], Γ^* is the photorespiratory compensation point (Pa), K is the effective Michaelis-Menten coefficient of Rubisco (Pa), η^* is the viscosity of water relative to its value at 25 °C, β is the ratio of cost factors for carboxylation and transpiration at 25 °C, c* is four times c, the unit cost of maintaining J_{max}. C_3 and C_4 vegetation were distinguished by the value for m, the CO_2 limitation term. While m is calculated as shown in Eq. (4) for C_3 vegetation, for C_4 plants m is assumed to be 1 due to the CO_2 concentrating mechanism[47].

A detailed description of the model can be found in Stocker et al.[15], where it is also showed that model can account for observed trends in GPP at multiple eddy-covariance flux sites. Soil water stress was implemented following Lavergne et al.[48], whereby χ is down-regulated under water stress via β following an empirical relationship with θ given as:

$$\ln\beta = 1.81\theta + 4.4 \quad (5)$$

A dynamic C_4 vegetation fraction was simulated, based on a C_3/C_4 competition model that uses the P model to predict C_3 and C_4 GPP[49]. Areas where cropland cover is higher than 50% were excluded in the C_4 vegetation fraction map. All calculations and analyses were conducted in the open-source environments R (version 4.1.2) and Python (version 3.10).

Environmental data

We downloaded globally averaged monthly mean CO_2 concentrations (μmol mol^{-1}) from the NOAA Global Monitoring Laboratory for 2000–2017 (NOAA/GML; https://gml.noaa.gov/ccgg/trends/; last access June 2022). Monthly precipitation, maximum, minimum and mean temperature and water vapour pressure at 0.5° resolution were derived from the Climate Research Unit (CRU) TS4.04 data set[50]. Vapour pressure deficit (VPD) was calculated using maximum, minimum temperature and water vapor pressure. Atmospheric pressure was estimated with global gridded elevation at 0.5° resolution in the WFDEI meteorological forcing dataset[51]. Hourly surface downwelling shortwave radiation was downloaded from the WFDE5 dataset version 2.0[52] and summed to provide monthly totals.

The CRU and WFDE5 data sets have relatively low spatial resolution and are consequently less suitable for site-level model evaluation. We obtained high-resolution climate data from the Climatologies at High resolution for the Earth's Land Surface Areas (CHELSA) dataset[53] and used this as the climate forcing at the site scale. The CHELSA data set provides monthly air temperature, precipitation, solar radiation, vapour pressure deficit data, with a spatial resolution of 30 arc sec (around 1 km)[53].

Root-zone soil moisture from the Global Land Evaporation Amsterdam Model (GLEAM) v3.6a product[54,55] available for the period 1980–2021 was used to estimate soil water stress on stomatal limitation of photosynthesis.

Annual tree cover percentages for 2000–2020 were derived from MODIS MOD44B v006[56]. Cropland cover at 0.05° resolution from 2001–2016 was derived from MODIS MCD12C1 v006[57] and regridded to 0.5° resolution using the first order conservative remapping function (*remapcon*) from the Climate Data Operators (CDO) software package (https://code.mpimet.mpg.de/projects/cdo).

Prediction of annual maximum vegetation cover

We hypothesize that on annual and longer time scales, the allocation of carbon to foliage is limited either by water supply, as a transpiring canopy cannot be sustained if insufficient root-zone water leads to prolonged stomatal closure; or by photosynthesis, as building and maintain leaves (and supplying them with water and nutrients) implies a carbon cost that cannot for long exceed the rate at which they fix carbon. We refer to these two cases as 'water limited' and 'energy limited'. Under water limitation, we hypothesize that plants collectively adjust their rooting behaviour to extract a fraction of annual precipitation from the soil, regardless of its distribution through the year, and allocate carbon to leaves in such a way that all of this water is transpired and GPP consequently maximized. Under energy limitation, we hypothesize that plants allocate carbon to leaves in such a way as to maximize GPP after subtracting the costs on constructing and maintain leaves and keeping them supplied with water and nutrients. This criterion leads to a well-defined optimum because investment in leaf tissue produces a diminishing return, due to the mutual shading of leaves.

General expressions for GPP and transpiration are:

$$A = G_s c_a (1 - \chi) = fAPAR . A_0 \quad (6)$$

and

$$E = 1.6\, G_s\, D \quad (7)$$

where A is GPP (we neglect leaf respiration for simplicity), A_0 is potential GPP assuming full vegetation coverage (fAPAR=1), E is transpiration, and G_s is the canopy conductance for CO_2. If we also assume that $E = f_0 P$ then re-arrangement immediately yields Eq. (1) as the water-limited fAPAR. We now define the net carbon profit (P_n) as:

$$P_n = fAPAR . A_0 - z . LAI \quad (8)$$

and assume Beer's Law:

$$fAPAR = 1 - \exp(-k . LAI) \quad (9)$$

Then

$$P_n = fAPAR . A_0 + \left(\frac{z}{k}\right)\ln(1 - fAPAR) \quad (10)$$

and

$$\frac{\partial P_n}{\partial(fAPAR)} = A_0 - \frac{\frac{z}{k}}{1 - fAPAR} \quad (11)$$

Setting Eq. (11) to zero yields Eq. (2), corresponding to a maximum in P_n. The minimum of energy-limited fAPAR ($fAPAR_c$) and water-limited fAPAR ($fAPAR_w$) was smoothly approximated using the log-sum-exp function (see text S1 for detailed derivation):

$$\min\{fAPAR_c, fAPAR_w\} \approx -\frac{1}{K}\log\left[\exp\left(-K.fAPAR_c\right) + \exp\left(-K.fAPAR_w\right)\right] \quad (12)$$

where K (≥1) is a constant. The larger the value for K, the closer the approximation is to minimum function (here we adopted K = 10). in our simulation. $fAPAR_w$ and $fAPAR_c$ were expressed as Eqs. (1) and (2) respectively. With $fAPAR_w$ and $fAPAR_c$ defined by Eqs. (1) and (2) respectively, we fitted values for f_0 and z using non-linear regression (*nls* function in R). The globally fitted values for z and f_0 were 13.86 mol m^{-2} a^{-1} and 0.62 (unitless) respectively.

Evaluation of predicted vegetation cover and its trend

We used remotely sensed products to evaluate our predictions at a global scale, as only remote sensing can provide the spatial and temporal continuity of data required for this purpose. We evaluated the modelled global fAPAR using the 0.05° resolution fAPAR data[58] at daily timestep from 2000–2017 derived from MODIS MOD15A2H Leaf Area Index/FPAR product[23]. The annual maximum fAPAR values were derived first by selecting the maximum value through the year, and then the 95th percentile of each set of 10 × 10 0.05° grid cells was used as the maximum fAPAR of each 0.5° grid cell.

To compare the performance of our framework with state-of-the-art dynamic global vegetation models, we downloaded LAI over 2000–2017 as simulated by the ensemble of 15 TRENDY[24] ecosystem models (TRENDY-v9; Tab. 1) (note that the models do not report fAPAR and generally do not model it separately from LAI). We used the S2 simulations, in which identical, time-varying climate and CO_2 are prescribed to all the models. TRENDY annual maximum LAI was taken as the maximum LAI value in a year in each grid cell and converted to $fAPAR_{max}$ using Eq. (9) for compare with modelled $fAPAR_{max}$.

We visually compared the multi-year average of modelled and observed fAPAR during 2000–2017 across the globe and evaluated the predicted $fAPAR_{max}$ using R-squared (R^2) and root mean squared error (RMSE). We also performed ordinary least-squares linear regression of observed versus predicted $fAPAR_{max}$.

Trends of global annual maximum fAPAR over the study period (2000–2017) were quantified using Mann-Kendall coefficients after regridded via CDO remapcon to a coarser resolution of 1.5° in order to reduce the incidence of false (positive or negative) trends. Areas with high values in the initial year ($fAPAR_{max}$ >0.85) were excluded to avoid near-zero trends. Besides MODIS fAPAR data, we also considered remotely-sensed greenness trends over the same period in the GEOV2[59], GLOBMAP[60] and AVHRR[61] products. We retained only those grid cells where at least three out of four products showed trends with the same sign. Predicted (MODIS) and observed trend coefficients were then compared in the same way as the predicted and observed fAPARmax.

We used both quadratic polynomials and bent-cable piecewise linear regression to detect whether there had been a shift in the fAPAR trend during the study period[43]. We conducted these analyses on each grid cell, and on the global average of modelled seasonally maximum fAPAR ($fAPAR_{max}$). The quadratic regression was compared to linear regression using ANOVA to determine whether a trend with a turning point could better describe the temporal pattern of fAPAR than a linear trend. Bent-cable regression allowed us to further classify heterogeneous fAPAR trends as being either cup-shaped, where a negative fAPAR trend ("browning") was followed by a positive trend ("greening"), or hat-shaped, where fAPAR at first increased but then declined. We constrained the turning points (where fAPAR trend shifts) to be in the middle 70% of the time series (2003–2014), following Higgins et al.[43].

In situ measurements provided additional evaluation of model performance. A total of 222 site-year LAI measurements were obtained from the Ground-Based Observations for Validation (GBOV) dataset in the Copernicus Global Land Products (https://gbov.acri.fr), and the OLIVE ground database[21,62]. The GBOV dataset is part of the Copernicus Global Terrestrial Service. Its purpose is to develop and distribute reliable in situ datasets from selected ground-based monitoring sites for systematic and quantitative validation of terrestrial products. The OLIVE dataset collects and processes ground-based measurements in accordance with CEOS-LPV guidelines to ensure data quality and consistency. The dataset includes shrubland, evergreen and deciduous broadleaf forests, needle leaves forests, and mixed forests, and spans the years 2000 through 2017. Combining the two datasets provides a broader range of representative biome types (as shown in Fig. S7). fAPAR was estimated from LAI with Eq. (9). For comparability with the modelled peak vegetation growth, we determined the annual maximum fAPAR as the peak greenness and evaluated the predicted against the observed $fAPAR_{max}$ using R^2 and RMSE. We determined the annual maximum fAPAR as the fAPAR at peak greenness, and evaluated the predicted against observed fAPARmax at the ground sites using R^2 and RMSE.

Sensitivity tests

For simplicity in our main analysis, we fitted a single, global value for each of the parameters z and f_0 across all grid cells and years. In principle, however, both z and f_0 could vary with environment. To assess the possibility of systematic variation with temperature, we divided the gridded climatologies into 5° average growing season temperature bins with a 1° moving window and fitted z and f_0 within each temperature bin.

A constant value of 0.5 for the light extinction coefficient (k) was adopted in our main analysis for the interconversion of fAPAR and LAI. As this coefficient is expected to vary with canopy structure, sensitivity tests were performed. We first calculated "apparent" values for k (assuming Beer's Law) from the multiyear average of MODIS annual maximum LAI and fAPAR during 2000–2017 (Fig. S3), and applied the resulting, spatially varying k in our log-sum-exp regression. We also compared this spatially varying k to MODIS land cover type and identified the median value of k within each major biome (Tab. S1). In an alternative approach, we used in situ measured mean growing-season values for k derived from a meta-analysis[40] (Tab. S1). The fitted values for f_0 and z under these different values for k were shown in Tab. S2, where the variation in k has a slight effect of values for z, but nearly no effect on f_0. The performance of the different fAPAR predictions was evaluated using R^2 and RMSE (Fig. S4).

Determination of drivers of the observed trends

To investigate the causes of LAI trends during the study period, we conducted simulations in which each one of the environmental variables (temperature, solar radiation, precipitation, soil moisture and CO_2 level) in turn was held constant at the value of initial year while other variables were allowed to change. The trends in $fAPAR_{max}$ derived from these factorial experiments at each grid cell were compared to the trends seen in the original simulation with all factors varying. The variable that produced the highest change in the trend was considered to be the factor controlling the trend. We also examined if this factor had a positive or negative impact on the $fAPAR_{max}$ trend by the sign of differences between factorial experiments and the original simulation.

Reporting summary

Further information on research design is available in the Nature Portfolio Reporting Summary linked to this article.

Data availability

Data used to reproduce all the figures in this research are published openly on Zenodo (https://zenodo.org/records/14283700) (https://doi.org/10.5281/zenodo.14283699).

Code availability

Code used to reproduce all the figures in this research are publicly available from Github repository (https://github.com/Shirleycwj/annual_maximum_fAPAR).

Received: 23 July 2023; Accepted: 2 January 2025;
Published online: 10 January 2025

References

1. Parker, G. G. Leaf Area Index (LAI) is both a determinant and a consequence of important processes in vegetation canopies. *For. Ecol. Manag.* **477**, 118496 (2020).
2. Li, F. et al. Vegetation clumping modulates global photosynthesis through adjusting canopy light environment. *Glob. Chang. Biol.* **29**, 731–746 (2023).
3. Saitoh, T. M. et al. Examination of the extinction coefficient in the Beer–Lambert law for an accurate estimation of the forest canopy leaf area index. *For. Sci. Technol*. **8**, (2012).
4. Wei, Z. et al. Revisiting the contribution of transpiration to global terrestrial evapotranspiration. *Geophys. Res. Lett.* **44**, 2792–2801 (2017).
5. Pei, Y. et al. Evolution of light use efficiency models: Improvement, uncertainties, and implications. *Agric. For. Meteorol.* **317**, 108905 (2022).
6. Wang, H. et al. Towards a universal model for carbon dioxide uptake by plants. *Nat. Plants* **3**, 734–741 (2017).
7. Bloomfield, K. J., Stocker, B. D., Keenan, T. F. & Prentice, I. C. Environmental controls on the light use efficiency of terrestrial gross primary production. *Glob. Change Biol.* **29**, 1037–1053 (2022).
8. De Pury, D. G. G. & Farquhar, G. D. Simple scaling of photosynthesis from leaves to canopies without the errors of big-leaf models. *Plant Cell Environ* **20**, 537–557 (1997).
9. Bao, S. et al. Environment-sensitivity functions for gross primary productivity in light use efficiency models. *Agric. For. Meteorol.* **312**, 108708 (2022).
10. Guan, X., Chen, J. M., Shen, H. & Xie, X. A modified two-leaf light use efficiency model for improving the simulation of GPP using a radiation scalar. *Agric. For. Meteorol.* **307**, 108546 (2021).
11. Prentice, I. C. et al. Principles for satellite monitoring of vegetation carbon uptake. *Nat. Rev. Earth Environ*. 1–15. (2024)
12. Harrison, S. P. et al. Eco-evolutionary optimality as a means to improve vegetation and land-surface models. *New Phytol* **231**, 2125–2141 (2021).
13. Yang, J. et al. Applying the concept of ecohydrological equilibrium to predict steady state leaf area index. *J. Adv. Model. Earth Syst.* **10**, 1740–1758 (2018).
14. Zhu, Z. et al. Optimality principles explaining divergent responses of alpine vegetation to environmental change. *Glob Chang Biol* **29**, 126–142 (2023).
15. Stocker, B. D. et al. P-model v1.0: an optimality-based light use efficiency model for simulating ecosystem gross primary production. *Geosci. Model Dev.* **13**, 1545–1581 (2020).
16. Cai, W. & Prentice, I. C. Recent trends in gross primary production and their drivers: analysis and modelling at flux-site and global scales. *Environ. Res. Letters* **15**, 124050 (2020).
17. Tan, S., Wang, H., Prentice, I. C. & Yang, K. Land-surface evapotranspiration derived from a first-principles primary production model. *Environ. Res. Lett.* **16**, 104047 (2021).
18. Duursma, R. A. & Falster, D. S. Leaf mass per area, not total leaf area, drives differences in above-ground biomass distribution among woody plant functional types. *New Phytol* **212**, 368–376 (2016).
19. Fang, H., Baret, F. & Plummer, P. & Schaepmaan-Strub. An overview of global leaf area index (LAI): methods, products, validation, and applications. *Rev. Geophys.* **57**, 739–799 (2019).
20. Xin, Q. et al. A semiprognostic phenology model for simulating multidecadal dynamics of global vegetation leaf area index. *J. Adv. Model. Earth Syst.* **12**, e2019MS001935 (2020).
21. Ground-Based Observations for Validation (GBOV) of Copernicus Global Land Products (https://gbov.acri.fr).
22. Garrigues, S. et al. Validation and intercomparison of global Leaf Area Index products derived from remote sensing data. *J. Geophys. Res.* **113**, G02028 (2008).
23. Myneni, R., Knyazikhin, Y. & Park, T. MOD15A2H MODIS Leaf Area Index/FPAR 8-Day L4 Global 500m SIN Grid V006. NASA EOSDIS Land Processes DAAC (2015).
24. Sitch, S. et al. Recent trends and drivers of regional sources and sinks of carbon dioxide. *Biogeosciences* **12**, 653–679 (2015).
25. Zhu, Z. et al. Greening of Earth and its drivers. *Nat. Clim. Chang.* **6**, 791–795 (2016).
26. Chen, C. et al. China and India lead in greening of the world through land-use management. *Nat. Sustain.* **2**, 122–129 (2019).
27. Manzoni, S. et al. Optimal plant water-use strategies under stochastic rainfall. *Water Resour. Res.* **50**, 5379–5394 (2014).
28. Yang, Y., Donohue, R. J., McVicar, T. R. & Roderick, M. L. An analytical model for relating global terrestrial carbon assimilation with climate and surface conditions using a rate limitation framework. *Geophys. Res. Lett.* **42**, 9825–9835 (2015).
29. Wang, H. et al. Leaf economics fundamentals explained by optimality principles. *Sci. Adv.* **9**, eadd5667 (2023).
30. Gill, A. L. & Finzi, A. C. Belowground carbon flux links biogeochemical cycles and resource-use efficiency at the global scale. *Ecol. Lett*. **19**, 1419–1428.
31. Vicente-Serrano, S. M., McVicar, T. R., Miralles, D. G., Yang, Y. & Tomas-Burguera, M. Unravelling the influence of atmospheric evaporative demand on drought and its response to climate change. *Wiley Interdiscip. Rev. Clim. Change* **11**, e632 (2020).
32. Bassirirad, H. Kinetics of nutrient uptake by roots: responses to global change. *New Phytol* **147**, 155–169 (2000).
33. Ma, H. et al. The global distribution and environmental drivers of aboveground versus belowground plant biomass. *Nat. Ecol. Evol.* **5**, 1110–1122 (2021).
34. Hatton, T., Salvucci, G. D. & Wu, H. I. Eagleson's optimality theory of an ecohydrological equilibrium: Quo vadis? *Funct. Ecol.* **11**, 665–674 (1997).
35. Kerkhoff, A. J., Martens, S. N. & Milne, B. T. An ecological evaluation of Eagleson's optimality hypotheses. *Funct. Ecol.* **18**, 404–413 (2004).
36. Good, S. P., Moore, G. W. & Miralles, D. G. A mesic maximum in biological water use demarcates biome sensitivity to aridity shifts. *Nat. Ecol. Evol.* **1**, 1883–1888 (2017).
37. Chen, J. M., Menges, C. H. & Leblanc, S. G. Global mapping of foliage clumping index using multi-angular satellite data. *Remote Sens. Environ.* **97**, 447–457 (2005).
38. Monsi, M. Uber den Lichtfaktor in den Pflanzengesellschaften und seine Bedeutung fur die Stoffproduktion. *Jap. J. Bot.* **14**, 22–52 (1953).
39. White, M. A., Thornton, P. E., Running, S. W. & Nemani, R. R. Parameterization and sensitivity analysis of the BIOME–BGC terrestrial ecosystem model: Net primary production controls. *Earth Interact* **4**, 1–85 (2000).
40. Zhang, L., Hu, Z., Fan, J., Zhou, D. & Tang, F. A meta-analysis of the canopy light extinction coefficient in terrestrial ecosystems. *Earth Sci. Front.* **8**, 599–609 (2014).
41. Zhao, M. & Running, S. W. Drought-induced reduction in global terrestrial net primary production from 2000 through 2009. *Science* **329**, 940–943 (2010).
42. Yuan, W. et al. Increased atmospheric vapor pressure deficit reduces global vegetation growth. *Sci. Adv.* **5**, 1396 (2019).
43. Higgins, S. I., Conradi, T. & Muhoko, E. Shifts in vegetation activity of terrestrial ecosystems attributable to climate trends. *Nat. Geosci*. 1-7 (2023).

44. Winkler, A. J. et al. Slowdown of the greening trend in natural vegetation with further rise in atmospheric CO2. *Biogeosciences* **18**, 4985–5010 (2021).
45. Lindh, M., Falster, D. S., Zhang, L., Dieckmann, U. & Brännström, Å. Latitudinal effects on crown shape evolution. *Ecol. Evol.* **8**, 8149–8158 (2018).
46. Bernacchi, C. J., Pimentel, C. & Long, S. P. In vivo temperature response functions of parameters required to model RuBP-limited photosynthesis. *Plant Cell Environ* **26**, 1419–1430 (2003).
47. Sage, R. F., Sage, T. L. & Kocacinar, F. Photorespiration and the evolution of C4 photosynthesis. *Annu. Rev. Plant Biol.* **63**, 19–47 (2012).
48. Lavergne, A. et al. Impacts of soil water stress on the acclimated stomatal limitation of photosynthesis: Insights from stable carbon isotope data. *Glob. Change Biol.* **26**, 7158–7172 (2020).
49. Orme, C. D. L. et al. *pyrealm* [Computer software]. https://github.com/ImperialCollegeLondon/pyrealm (2023).
50. Harris, I., Osborn, T. J., Jones, P. & Lister, D. H. Version 4 of the CRU TS monthly high-resolution gridded multivariate climate dataset. *Sci. Data* **7**, 109 https://rdcu.be/b3nUI (2020).
51. Weedon, G. P. et al. The WFDEI meteorological forcing data set: WATCH Forcing Data methodology applied to ERA-Interim reanalysis data. *Water Res. Research* **50**, 7505–7514 (2014).
52. Cucchi, M. et al. Near surface meteorological variables from 1979 to 2019 derived from bias-corrected reanalysis, version 2.0. Copernicus Climate Change Service (C3S) Climate Data Store (CDS), https://doi.org/10.24381/cds.20d54e34 (2021).
53. Brun, P. et al. Global climate-related predictors at kilometre resolution for the past and future. *Earth Syst. Sci. Data* **14**, 5573–5603 (2022).
54. Martens, B. et al. GLEAM v3: satellite-based land evaporation and root-zone soil moisture. *Geosci. Model Dev.* **10**, 1903–1925 (2017).
55. Miralles, D. G. et al. Global land-surface evaporation estimated from satellite-based observations. *Hydro. Earth Sys. Sci.* **15**, 453–469 (2011).
56. DiMiceli, C. M. et al. MOD44B MODIS/Terra vegetation continuous fields yearly L3 global 250m SIN grid V006. In: NASA EOSDIS Land Processes DAAC. https://doi.org/10.5067/MODIS/MOD44B.006 (2015).
57. Friedl, M. & Sulla-Menashe, D. MCD12C1 MODIS/Terra+Aqua Land Cover Type Yearly L3 Global 0.05Deg CMG V006. In: NASA EOSDIS Land Processes DAAC, https://doi.org/10.5067/MODIS/MCD12C1.006 (2015).
58. Jiang, C. & Ryu, Y. Multi-scale evaluation of global gross primary productivity and evapotranspiration products derived from Breathing Earth System Simulator (BESS). *Remote Sens. Env.* **186**, 528–547 (2016).
59. Baret, F. et al. GEOV1: LAI and FAPAR essential climate variables and FCOVER global time series capitalizing over existing products. Part1: Principles of development and production. *Remote Sens Environ* **137**, 299–309 (2013).
60. Liu, Y. et al. Retrospective retrieval of long-term consistent global leaf area index (1981–2011) from combined AVHRR and MODIS data. *J. Geophys. Res. Biogeosci*. **117**, (2012).
61. Claverie, M. et al. A 30+ year AVHRR LAI and FAPAR climate data record: Algorithm description and validation. *Remote Sens* **8**, 263 (2016).
62. Baret, F. et al. Evaluation of the representativeness of networks of sites for the validation and inter-comparison of land biophysical products. *IEEE Trans. Geosc. Remote Sens.* **44**, 1794–1803 (2006).
63. Haverd, V. et al. A new version of the CABLE land surface model (Subversion revision r4601) incorporating land use and land cover change, woody vegetation demography, and a novel optimisation-based approach to plant coordination of photosynthesis. *Geosci. Model Dev.* **11**, 2995–3026 (2018).
64. Melton, J. R. et al. CLASSIC v1.0: the open-source community successor to the Canadian Land Surface Scheme (CLASS) and the Canadian Terrestrial Ecosystem Model (CTEM) – Part 1: Model framework and site-level performance. *Geosci. Model Dev.* **13**, 2825–2850 (2020).
65. Lawrence, D. M. et al. The Community Land Model Version 5: Description of new features, benchmarking, and impact of forcing uncertainty. *J. Adv. Model. Earth Sy.* **11**, 4245–4287 (2019).
66. Yuan, W. et al. Multiyear precipitation reduction strongly decreases carbon uptake over northern China. *J. Geophys. Res. Biogeo.* **119**, 881–896 (2014).
67. Meiyappan, P., Jain, A. K. & House, J. I. Increased influence of nitrogen limitation on CO2 emissions from future land use and land use change. *Global Biogeochem. Cy.* **29**, 1524–1548 (2015).
68. Delire, C. et al. The global land carbon cycle simulated with ISBA-CTRIP: Improvements over the last decade. *J. Adv. Model Earth Sy.* **12**, e2019MS001886 (2020).
69. Reick, C. H. et al. JSBACH 3 – The land component of the MPI Earth System Model: documentation of version 3.2. https://doi.org/10.17617/2.3279802 (2021).
70. Wiltshire, A. J. et al. JULES-CN: a coupled terrestrial carbon–nitrogen scheme (JULES vn5.1). *Geosci. Model Dev.* **14**, 2161–2186 (2021).
71. Smith, B. et al. Implications of incorporating N cycling and N limitations on primary production in an individual-based dynamic vegetation model. *Biogeosci* **11**, 2027–2054 (2014).
72. Lienert, S. & Joos, F. A Bayesian ensemble data assimilation to constrain model parameters and land-use carbon emissions. *Biogeosci* **15**, 2909–2930 (2018).
73. Zaehle, S. & Friend, A. D. Carbon and nitrogen cycle dynamics in the O-CN land surface model: 1. Model description, site-scale evaluation, and sensitivity to parameter estimates: Site-scale evaluation of a C-N model. *Global Biogeochem. Cy.* **24**, GB1005 (2010).
74. Vuichard, N. et al. Accounting for carbon and nitrogen interactions in the global terrestrial ecosystem model ORCHIDEE (trunk version, rev 4999): multi-scale evaluation of gross primary production. *Geosci. Model Dev.* **12**, 4751–4779 (2019).
75. Walker, A. P. et al. The impact of alternative trait-scaling hypotheses for the maximum photosynthetic carboxylation rate (Vcmax) on global gross primary production. *New Phytol* **215**, 1370–1386 (2017).
76. Kato, E. et al. Evaluation of spatially explicit emission scenario of land-use change and biomass burning using a process-based biogeochemical model. *J. Land Use* **8**, 104–122 (2013).
77. Yue, X. & Unger, N. The Yale Interactive terrestrial Biosphere model version 1.0: description, evaluation and implementation into NASA GISS ModelE2. *Geosci. Model Dev.* **8**, 2399–2417 (2015).

Acknowledgements

WC was funded by the Chinese Scholarship Council ((grant number 201908060024 to WC). ZZ and HW acknowledge support from the National Natural Science Foundation of China (72140005) and the Tsinghua University Initiative Scientific Research Program (20223080041). ICP acknowledges support from the European Research Council under the European Union's Horizon 2020 research and innovation programme (Grant Agreement No: 787203 REALM). YR was supported by National Research Foundation of Korea (NRF-2019R1A2C2084626). SPH acknowledges support from the ERC-funded project GC2.0 (Global Change 2.0: Unlocking the past for a clearer future, No. 694481). This research is a contribution to the Land Ecosystem Models based On New Theory, obseRvations and ExperimEnts (LEMONTREE) project funded through the generosity of Eric and Wendy Schmidt by recommendation of the Schmidt Futures program. All authors acknowledge support from LEMONTREE.

Author contributions

I.C.P., S.P.H., H.W. conceived the research; B.Z. first demonstrated the utility of the dual optimality criterion for peak LAI. W.C. and Z.Z. carried out the data processing and analyses; Y.R. provided corrected MODIS fAPAR data for analyses; all authors contributed to the interpretation of the results.

I.C.P. wrote the first outline of the paper, W.C. wrote the first complete draft, and all authors contributed to the final version.

Competing interests
The authors declare no competing interests.

Additional information
Supplementary information The online version contains supplementary material available at https://doi.org/10.1038/s43247-025-01992-0.

Correspondence and requests for materials should be addressed to Wenjia Cai.

Peer review information *Communications Earth & Environment* thanks the anonymous reviewers for their contribution to the peer review of this work. Primary Handling Editors: Jinfeng Chang and Martina Grecequet. A peer review file is available.